
Volume 298, Issues 3–4
1 October 2010
ISSN 0012-821X
ELSEVIER
EARTH
& PLANETARY
SCIENCE LETTERS
Editors
Rick Carlson, Washington, DC
Peggy Delaney, Santa Cruz, CA
Peter B. deMenocal, Palisades, NY
T. Mark Harrison, Los Angeles, CA
Yanick Ricard, Lyon
P. Shearer, La Jolla, CA
Tilman Spohn, Berlin
Lars Stixrude, London
Rob van der Hilst, Cambridge, MA

Earth and Planetary Science Letters 298 (2010) 306–316

Contents lists available at ScienceDirect

Earth and Planetary Science Letters

journal homepage: www.elsevier.com/locate/epsl

Temporal and spatial variation of stress field in Taiwan from 1991 to 2007: Insights from comprehensive first motion focal mechanism catalog

Yih-Min Wu [a,*], Ya-Ju Hsu [b], Chien-Hsin Chang [c], Louis Suh-yui Teng [a], Mamoru Nakamura [d]

[a] Department of Geosciences, National Taiwan University, Taipei, 106, Taiwan
[b] Institute of Earth Sciences, Academia Sinica, Taipei 115, Taiwan
[c] Central Weather Bureau, Taipei 100, Taiwan
[d] Department of Physics and Earth Science, University of the Ryukyus, Okinawa, Japan

ARTICLE INFO

Article history:
Received 16 July 2009
Received in revised form 26 July 2010
Accepted 29 July 2010

Editor: R.D. van der Hilst

Keywords:
earthquake
focal mechanism
stress
crustal deformation

ABSTRACT

The total amount of 4,761 focal mechanisms was determined based on P-wave first motion polarities from 1991 to 2007 in Taiwan region. This dataset offers us a good opportunity to examine temporal and spatial variability of the stress field. We find that the spatial variations of stress axes are mainly controlled by tectonic structures while the temporal changes are greatly influenced by the Chi-Chi earthquake. The orientation of the maximum horizontal compressive stress axes (S_H) shows a general agreement with the direction of plate motion between a depth range of 0–30 km. The 20° anticlockwise rotation of S_H from the Longitudinal Valley (LV) to western Taiwan is probably caused by the left-lateral motion on the Longitudinal Valley Fault (LVF) that has consumed part of the oblique motion of plate convergence. On the other hand, part of the oblique convergence is transferred into the Central Range and the Hsuehshan Range judging from counterclockwise rotation of S_H from east to west and strike-slip faulting in the Hsuehshan Range. Most events with a depth greater than 30 km occur offshore eastern Taiwan and the azimuth of S_H is close to E–W directed, different from NW–SE directed at shallow depths. This may infer the existence of the transition of lithosphere rheology in offshore eastern Taiwan. The trends of S_H in the depth of 0–10 km are strongly affected by the coseismic stress change of the Chi-Chi earthquake. In the northern half of the Chi-Chi rupture area, the trends of S_H rotate 30° clockwise and the stress ratio increased by a factor of six after the mainshock. The orientations of S_H still differ by 30° in 2007 comparing to that in the period before the Chi-Chi earthquake. The variation of S_H trend is more diverse in the southern half of the rupture area, showing 20° counterclockwise rotation immediately after the 1999 mainshock followed by a clockwise rotation. The trend of S_H returns to the pre-seismic direction of 110° in 2001. These notable changes of S_H before and after the Chi-Chi mainshock suggests that the magnitude of background stress in the rupture area is close to the coseismic stress drop. We also recognize a significant 10° counterclockwise rotation of S_H in the entire Chi-Chi rupture area between 1991 and 1999 before the earthquake took place. However, to the south of the Chi-Chi rupture, the trends of S_H remain little changed before and after the Chi-Chi earthquake.

1. Introduction

Taiwan is one of the most seismically active regions in the world. It is situated in the western portion of the Pacific Rim seismic belt. The Philippine Sea Plate (PSP) subducts northward under the Eurasian Plate (EP) along the Ryukyu trench offshore eastern Taiwan. Off the southern tip of the island, the EP subducts eastward under the PSP (Tsai et al., 1977; Wu et al., 2009a,b). As a result of the regional tectonic motion, most of Taiwan is under a northwest–southeast contraction with a convergence rate of about 80 mm/year (Hsu et al., 2009a; Yu et al., 1997). The Taiwan orogen, formed by the collision of the Luzon Arc with the China continent in the past 5–6 My (Huang et al., 2006; Teng, 1990), is relatively young on the geological timescale. The island is characterized by a high shortening rate and a strong seismic activity. Since 1994, the Central Weather Bureau Seismic Network (CWBSN) has recorded about 18,000 events each year in a roughly 400 km × 550 km region (Shin et al., 2003; Wu et al., 2008a). The CWBSN consists of 71 real-time seismic stations in Taiwan region (Fig. 1). Furthermore, 715 strong motion stations from the Taiwan Strong Motion Instrumentation Program (TSMIP) and 13 seismic stations from the Japan Meteorological Agency (JMA) were deployed around the Taiwan region. The distribution of seismic stations provides a nice spatial coverage for earthquake monitoring.

* Corresponding author. No. 1, Sec. 4th, Roosevelt Road, Department of Geosciences, National Taiwan University, Taipei, Taiwan. Tel.: +886 2 2362 0054; fax: +886 2 2364 4625.
E-mail address: drymwu@ntu.edu.tw (Y.-M. Wu).

0012-821X/$ – see front matter © 2010 Elsevier B.V. All rights reserved.
doi:10.1016/j.epsl.2010.07.047

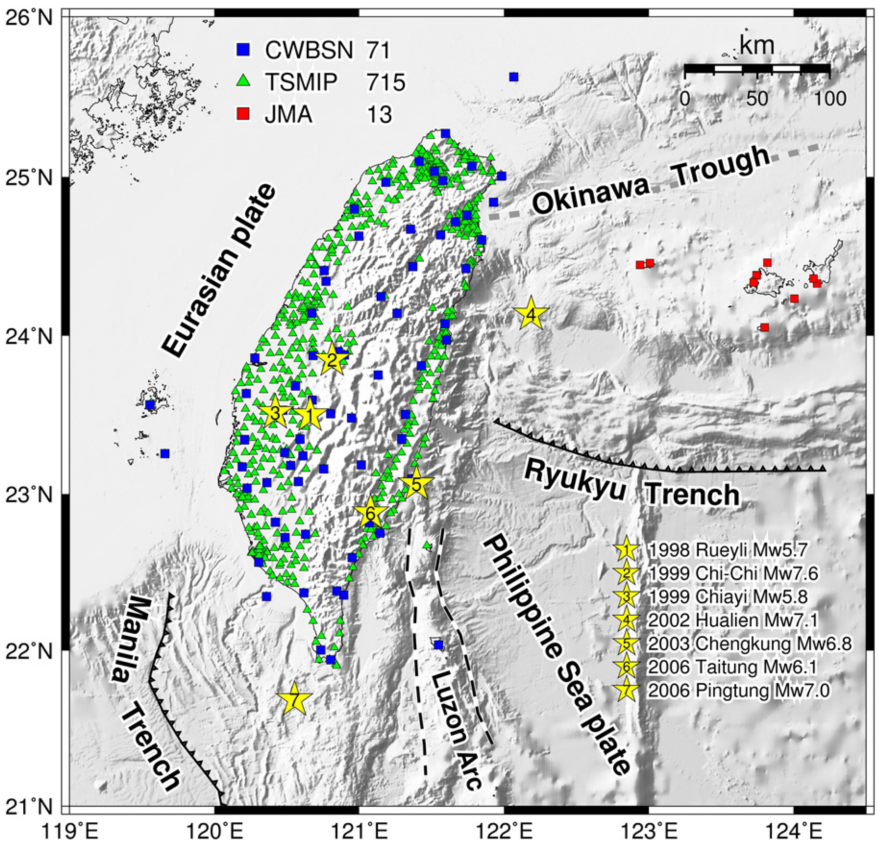

Fig. 1. Distribution of seismic stations from different networks (CWBSN, TSMIP, and JMA). Stars with number show the epicenters of damaging events in the study periods in Taiwan.

Many devastating earthquakes which have occurred in the past decade have been well-recorded and carefully studied, for example, the 1998 Rueyli M_w5.7 earthquake (Chen et al., 1999; Wu et al., 2003), the 1999 Chi-Chi M_w7.6 earthquake (e.g., Chang et al., 2000, 2007; Chen et al., 2006; Hsu et al., 2009b; Shin and Teng, 2001; Teng et al., 2001; Wu and Chen, 2007; Wu and Chiao, 2006), the 1999 Chiayi M_w5.8 earthquake (Chang and Wang, 2006; Chen et al., 2008), the 2002 Hualien M_w7.1 earthquake (e.g., Chen et al., 2004), the 2003 Chengkung M_w6.8 earthquake (e.g., Hsu et al., 2009c; Hu et al., 2007; Wu et al., 2006a), the 2006 Taitung M_w6.1 earthquake (e.g., Chen et al., 2009; Wu et al., 2006b), and the Pingtung M_w7.0 earthquake in December 2006 (e.g., Wu et al., 2009b). The abundant earthquakes and well-recorded data in Taiwan provide a valuable database to study both the lithosphere structure and earthquake sources.

Accurate and reliable earthquake information is fundamental to many seismological studies. In the past few years, we have been working on a basic earthquake database in the Taiwan region for related earthquake researches. First, we obtained the regional 3-D P-wave and Vp/Vs structures by combining a large dataset of S-P times from the TSMIP records with the P- and S-wave arrival times from the CWBSN, JMA, and some temporary ocean bottom seismograph (OBS) stations (Wu et al., 2007, 2009a,b). Second, the earthquake hypocenters of the Taiwan region are relocated using three-dimensional velocity model (Wu et al., 2008a). The focal mechanisms of moderate-size earthquakes ($M_L \geqq 4.0$ from 1991 to 2005) are determined using genetic algorithm (GA) method (Wu et al., 2008b).

Earthquake focal mechanisms can provide information about the regional stress patterns and seismotectonic environments. A complete focal mechanism catalog can also be useful in other studies such as waveform tomography as well as earthquake source mechanism analysis. Although focal mechanisms of moderate-size earthquakes were determined by our previous study (Wu et al., 2008b), that dataset lacked small earthquakes to provide a better coverage in time and space. In this study, we analyzed all the earthquakes from 1991 to 2007 in the Taiwan region to offer a comprehensive dataset of focal mechanism and conducted stress tensor inversions. The number of events in the new dataset is about three times that in Wu et al. (2008b). In addition, the P-wave polarities from JMA stations of the Ryukyu region are used to give a better spatial coverage for events in offshore northeast Taiwan compared to our previous study.

2. Data and analysis

First motion polarities from the CWBSN, TSMIP, and JMA are used in this study to determine focal mechanisms. The P-wave polarities of the CWBSN are read from CWBSN catalog and those from the TSMIP and JMA stations are picked in this study. We use the total amounts of 44,847 and 5,419 first motion polarities from TSMIP and JMA, respectively. Three-dimensional earthquake locations were applied to the entire CWBSN catalog earthquakes using P and S arrivals from CWBSN and JMA as well as S-P time from the TSMIP (Wu et al., 2007, 2009a). A GA method (Wu et al., 2008b) was used to determine focal mechanisms of all earthquakes.

A total of 4,761 focal mechanisms were determined from 1991 to 2007 in the Taiwan region (Fig. 2 and Table 1 as the supplementary material). Fig. 3 shows the statistics of focal mechanisms including time, magnitude (M_L), and depth distributions. Focal depths of those events range from 1 to 143 km with the majority occurring at shallow depths of less than 20 km. The average depth is 20 km with a standard deviation of 18 km. The magnitudes vary between 1.8 and 7.3 with an average of 3.9 ± 0.7. Based on this distribution, the magnitude completeness of this catalog should be around 3.5 to 4.0. The number

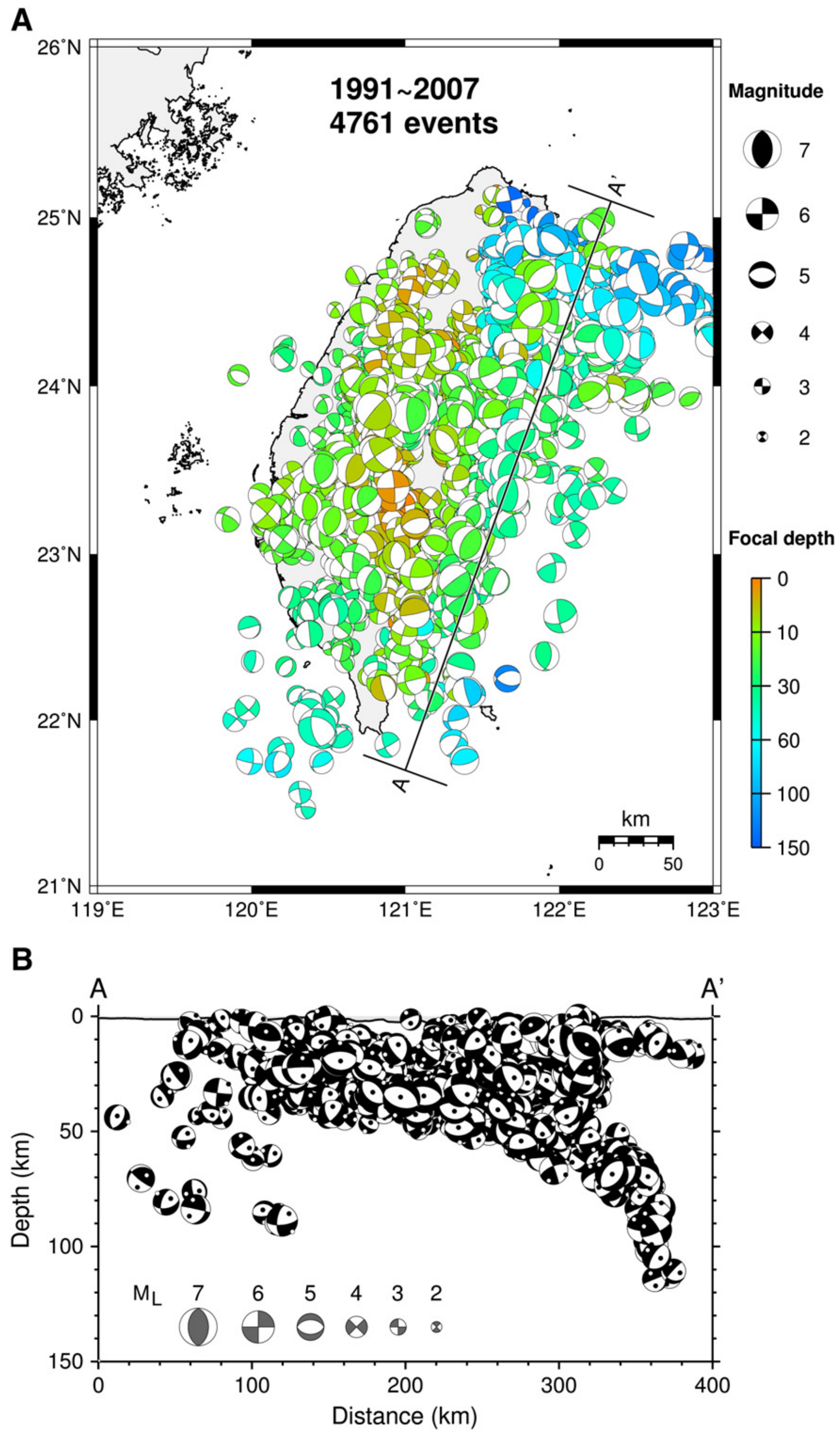

Fig. 2. A. Distribution of focal mechanisms determined in this study from 1991 to 2007. AA′ shows the location of the profile in Figure 2B. B. A NE–SW transect of earthquake focal mechanisms.

of events significantly increases after the 1999 Chi-Chi earthquake but returns to the background value of about 200 events per year in 2002.

Compared to the old dataset (Wu et al., 2008b), the new dataset provides more focal mechanisms to investigate temporal and spatial variations of the regional stress field. It allows us to examine the influence of the Chi-Chi earthquake on the pattern of stress orientations using the stress tensor inversion method proposed by Michael (1984, 1987). Their method finds the optimal stress tensor that minimizes the difference between the trend of the shear traction on the fault plane and the fault slip direction for a population of earthquakes. In order to find a continuous variation of stress orientations in space, we use a moving-window inversion on the 0.25°-spacing grid and include all events within a 0.5° × 0.5° rectangle centered at the node. We estimate the stress tensor only when there are at least 10 earthquakes within a given rectangular box. The main results are shown in the following sections.

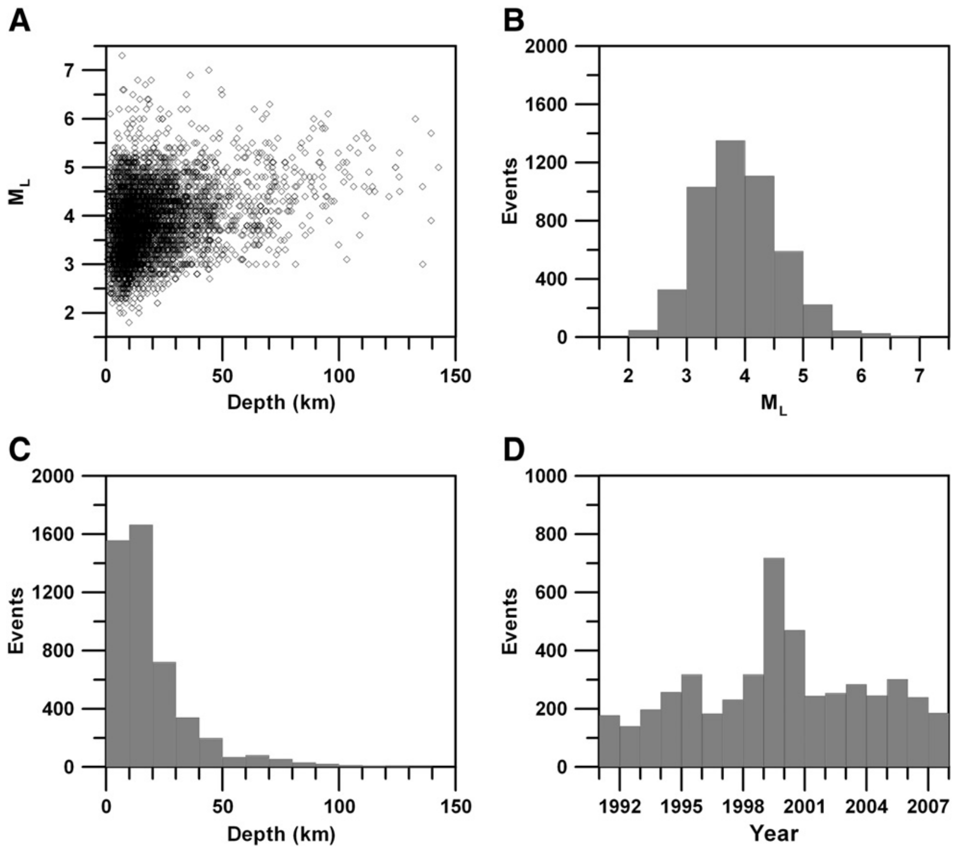

Fig. 3. Statistics of focal mechanisms. (A) The earthquake magnitude as a function of focal depth. (B to D) show number of events as a function of magnitude, focal depth and time, respectively.

3. Spatial variations of stress orientations

Wu et al. (2008b) delineate orientations of principal stress axes using all focal mechanisms in the crust with a depth of less than 30 km before the Chi-Chi earthquake. With much more focal mechanisms available in this study, we were able to examine variations of stress orientations at four depth profiles ranging from 0 to 10 km, 10 to 20 km, 20 to 30 km, and 30 to 50 km. We show the trends of maximum horizontal compressive axes (S_H) with one standard deviation before and after the Chi-Chi earthquake in Figs. 4 and 5, respectively. The direction of S_H corresponding to the direction of the normal of the vertical plane experiencing maximum normal stress, which is calculated using the method proposed by Lund and Townend (2007).

Before the Chi-Chi earthquake, the trends of S_H at shallow depths of 0–10 km smoothly varied from 130° in the LV to 110° near the Coastal Plain in western Taiwan (Fig. 4A). The directions of S_H axes in the entire LV are roughly consistent from the surface to 10 km deep. At the depth range of 10–20 km, the trends of S_H indicate sharp variations in space. In SW Taiwan and southern LV, where surface deformation is characterized by strong horizontal shortening based on GPS data (Hsu et al., 2009a), the trends of S_H rotate about 20° anticlockwise corresponding to those at shallow depths (Fig. 4B). The directions of S_H in northern LV show a coherent trend of about 130° at the depth range between the surface and 20 km, while the azimuth of S_H rotates 10° counterclockwise at the depth between 20 and 30 km and become E–W-oriented deeper than 30 km (Fig. 4CD). Most events with depths greater than 30 km occur in offshore eastern Taiwan, where the azimuth of S_H is about 105° (Fig. 4D).

Kao et al. (1998) inferred that strain partitioning occurred to the east of the LV and found that the P axes of focal mechanisms offshore eastern Taiwan (23–24°N, ~121.9°E) can be divided into two groups, 287° ± 10° and 333° ± 16°. We find that this variation is possibly not at horizontal space but rather in the depth. The azimuths of P axes (very close to orientations of S_H) shallower than 20 km are roughly consistent with the direction of plate motion (corresponding to the second group of 333° ± 16° in Kao et al., 1998), while P axes rotate anticlockwise to be more E–W-directed at deep depths (corresponding to the group of 287 ± 10° in Kao et al., 1998). This implies that the stress partitioning is probably due to rheological change at depth near the east coast.

The trends of S_H estimated from focal mechanisms after the Chi-Chi Earthquake are shown in Fig. 5. The primary variations of the S_H orientations before and after the mainshock reside in the depth range of 0–10 km. In central Taiwan, the S_H directions show systematic clockwise rotations of 15° in the Western Foothills (~120.8°E/24°N) and of 35° to the north of the LV (~121.6°E/24°N) after the mainshock (Fig. 5A). Results from stress tensor inversions show N–S compression beneath the Coast Plain in the depth range of 0–20 km (Fig. 5AB). Similar phenomena can be found in the Chi-Chi rupture area at 20–50 km depth (Fig. 5CD). Note that the occurrence of the 2006 Pingtung earthquake induced a series of aftershocks with S_H trending 140° in SW Taiwan as shown by the stress tensor inversion using about 15 focal mechanisms in the depth range of 30–50 km (Fig. 5D).

4. Temporal variations of stress orientations near the Chi-Chi rupture area

We divide the rupture area of the Chi-Chi earthquake into three regions, *A*, *B* and *C*, as indicated in Fig. 6. Boxes *A* and *B* cover the northern half and southern half of the Chi-Chi rupture area, respectively. The boundary between Boxes *A* and *B* is decided

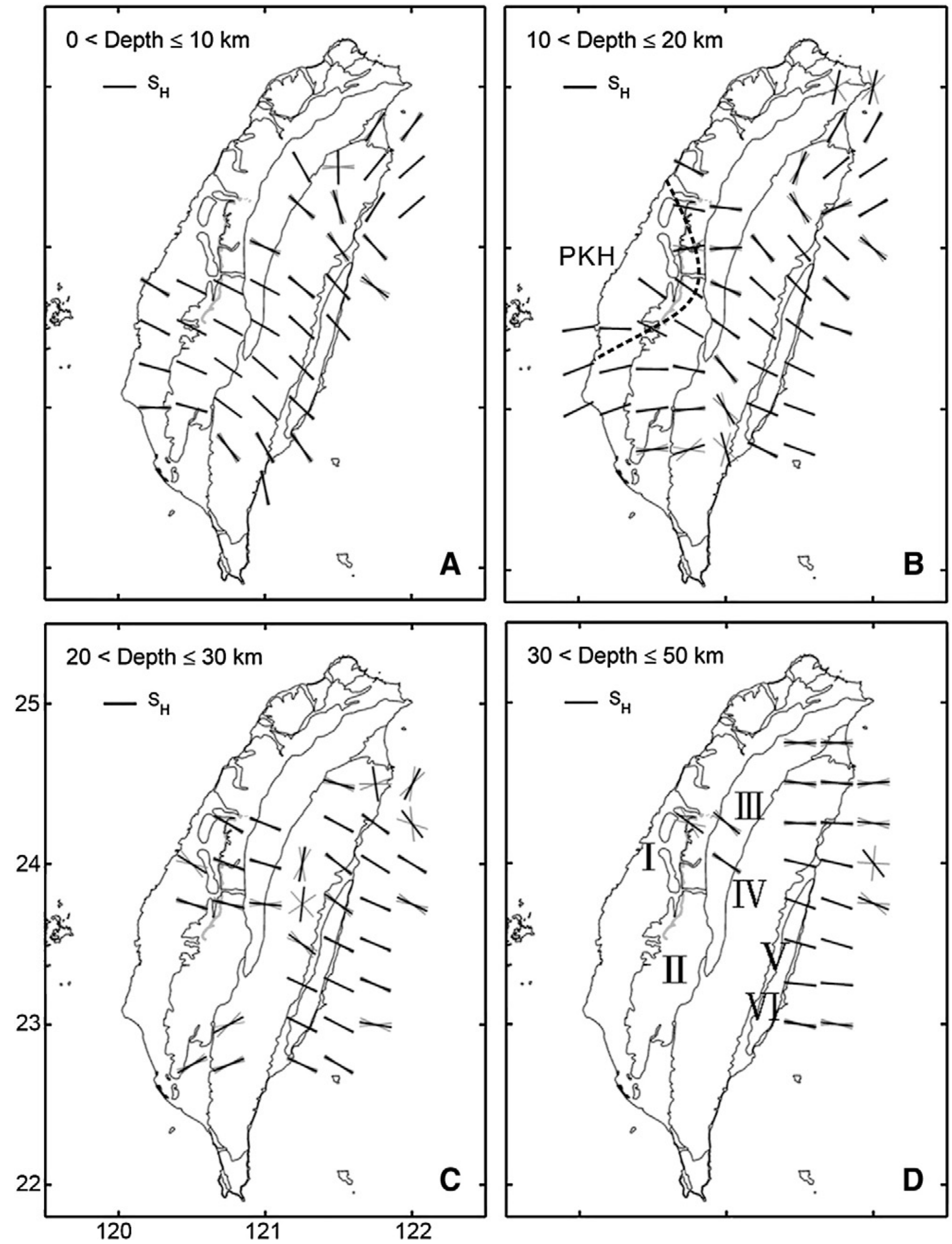

Fig. 4. Orientations of maximum horizontal compressive stress (S_H) before the Chi-Chi earthquake at four depth ranges of (A) 0–10 km (B) 10–20 km (C) 20–30 km and (D) 30–50 km. The outline of Peikang basement high (PKH) is indicated as a black dashed line in (B). The major geological units in Taiwan are indicated in (D). I: Coastal Plain. II: Western Foothills. III: Hsueshan Range. IV: Central Range. V: Longitudinal Valley. VI: Coastal Range. Grey line indicate one standard deviation of the trend of SH. The outline of Peikang basement high (PKH) is indicated as a black dashed line in (B).

according to the faulting style which will be described in the next section. The region in Box *C* contains the region to the south of the rupture zone. All three boxes have the same spatial size.

The stress tensor inversion at each box is performed using all earthquake focal mechanisms with focal depths less than 30 km. We conduct stress tensor inversions using all events before (1991–1999.7) and after (1999.7–2008) the Chi-Chi earthquake, respectively (Fig. 6). The trend of S_H and stress ratio ($R = \frac{\sigma_2 - \sigma_3}{\sigma_1 - \sigma_3}$) are shown in Fig. 6. The fault types are between thrust faulting and strike-slip faulting in *A* and *B* with a small *R* value of about 0.1 to 0.2 implying slight transpression before the Chi-Chi earthquake. Box *C* shows a predominantly strike-slip faulting with $R = 0.4$ and the intermediate stress axis (σ_2) close to vertical. The trends of S_H are 100°, 106° and 119° from northern to southern boxes, respectively. After the Chi-Chi earthquake, the fault types are dominated by strike-slip faulting in Box *A* and thrust faulting in Box *B*, respectively. The trends of S_H rotated about 25° in Box *A*, while they remain unchanged in Box *B* and *C*. Moreover, the stress ratio, *R*, increases by a factor of six in Box *A*. The dramatic change of stress status in Box *A* is related to the large coseismic slip of more than 10 m (Hsu et al., 2009b) and the amplitude reduction of maximum principal stress after the mainshock.

Mozziconacci et al. (2009) found a 25° clockwise rotation of the σ_1 axis between pre- and post–Chi-Chi periods in the area near the northern termination of the coseismic rupture, which is consistent with the 25° clockwise rotation of S_H in our study, although the methods of determining focal mechanisms and stress tensor inversions are different.

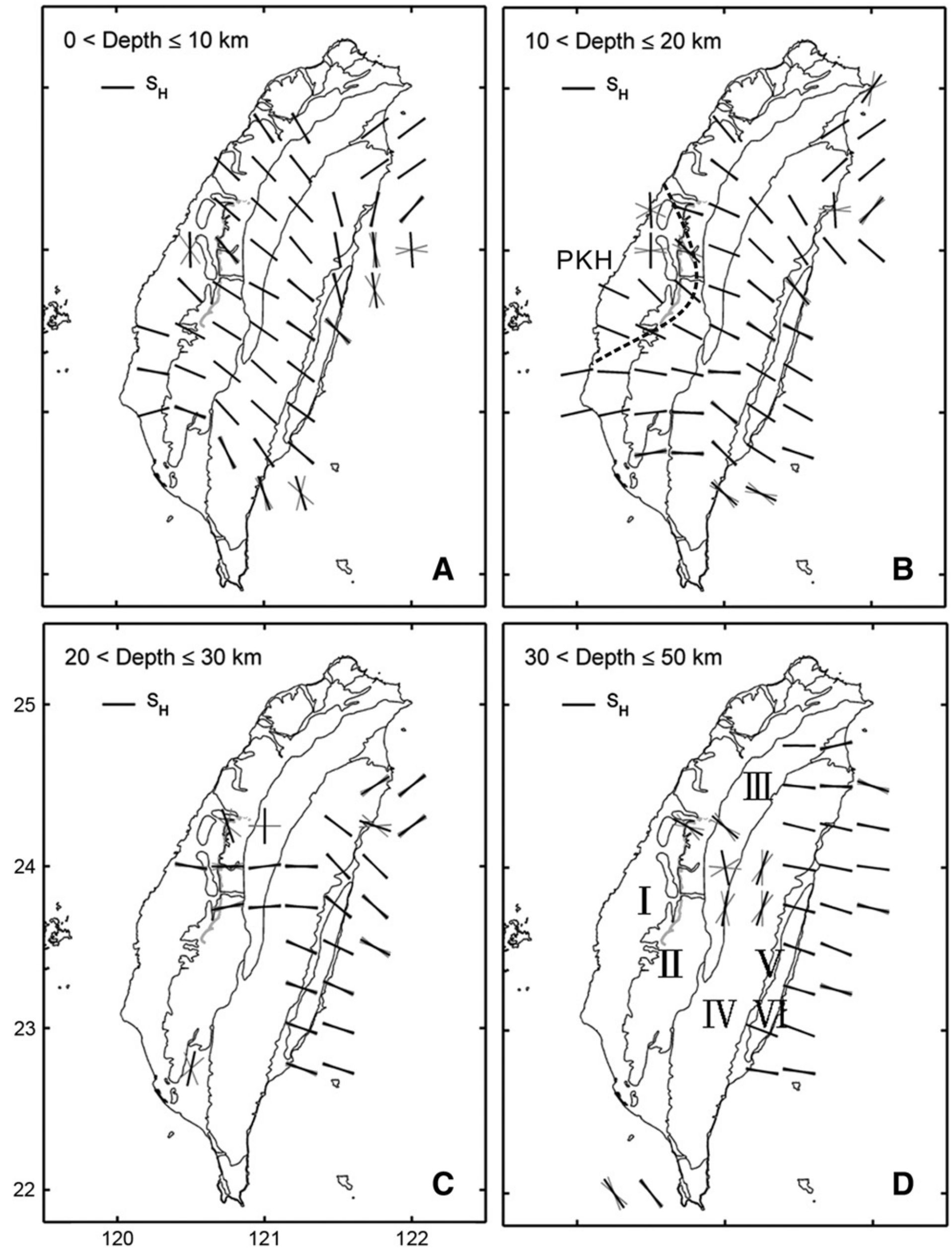

Fig. 5. Orientations of maximum horizontal compressive stress (S_H) after the Chi-Chi earthquake at four depth ranges of (A) 0–10 km (B) 10–20 km (C) 20–30 km and (D) 30–50 km. The major geological units in Taiwan are indicated in (D). I: Coastal Plain. II: Western Foothills. III: Hsueshan Range. IV: Central Range. V: Longitudinal Valley. VI: Coastal Range. Grey line indicate one standard deviation of the trend of SH. The outline of Peikang basement high (PKH) is indicated as a black dashed line in (B).

5. Temporal variations of stress orientations in central Taiwan

Since our new dataset contains abundant focal mechanisms (Fig. 6), we are able to conduct stress tensor inversions in multiple time windows and examine temporal evolutions of stress orientations in this study.

We divide earthquake focal mechanisms before the Chi-Chi earthquake in central Taiwan into three equal time windows between 1991 and 1999.7. The focal mechanisms after the mainshock are divided into six time periods as 0–1 month, 1–4 months, 4–10 months, 10–22 months, 22–46 months, and 46–94 months afterward. These time windows are partitioned by taking into account the logarithmic decay of seismicity after the mainshock (Perfettini and Avouac, 2004).

The orientations of S_H is stationary between 1991 and 1996.8 in the northern half of the Chi-Chi rupture area (Box *A*); while the trend of S_H rotates 10° counterclockwise in the period between 1996.8 and 1999.7 (Fig. 7). Right after the Chi-Chi earthquake, S_H rotated 30° clockwise. Between 2003 and 2007, S_H trended 130°, about 30° different from the pre-seismic orientation.

The stress tensor inversions in the southern half of the Chi-Chi rupture zone (Box *B*) show that orientations of principal stress axes are roughly stationary and the average trend of S_H is about 110° between 1991 and 1999.7. However, there is a 10° counterclockwise rotation of S_H between 1991 and the Chi-Chi mainshock. The S_H orientations varied considerably in the first year after the mainshock, but returned to the pre-seismic direction after 2001 (Fig. 8).

To the south of the Chi-Chi rupture area (Box *C*), the strike-slip and thrust faulting mechanisms prevail both before and after the mainshock (Figs. 6 and 9), with S_H varied slightly about 120°. Though the influence of the Chi-Chi earthquake on the stress regime is indistinct, a clear NW-SE alignment of seismicity was induced (Fig. 6B), which is not observed before (Fig. 6A).

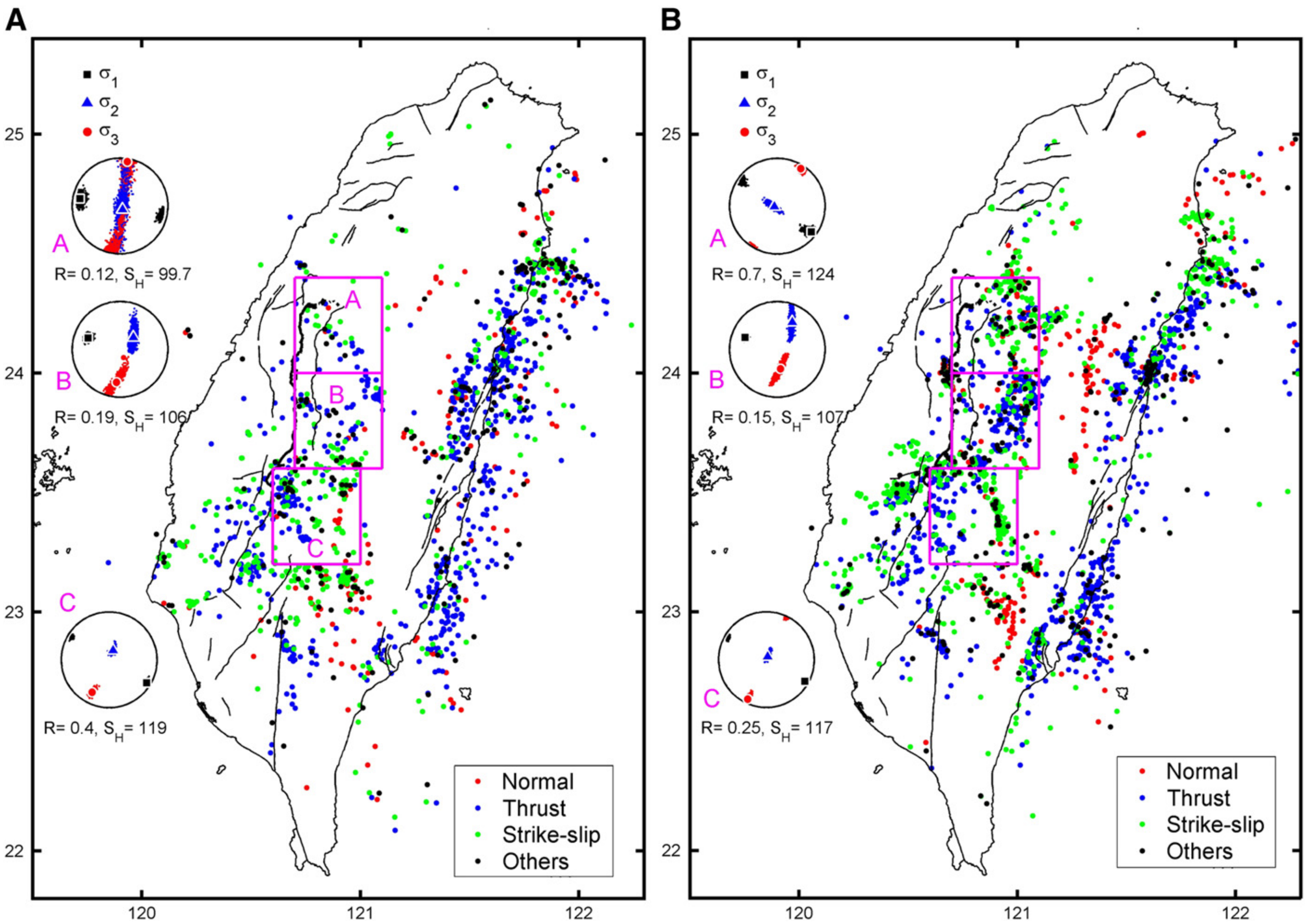

Fig. 6. Fault types in Taiwan and stress tensor inversions in the Chi-Chi rupture area (A) before and (B) after the Chi-Chi earthquake using events with focal depths of less than 30 km. The focal mechanisms are divided into four categories, including normal, thrust, strike-slip faulting and others (Frohlich, 2001) and indicated as colored dots. The results of stress tensor inversions in three regions, *A*, *B* and C, are shown on the left of each panel. Squares, triangles, and circles represent three principal stress axes, σ_1, σ_2 and σ_3, in equal-area projection of the lower hemisphere. The best solutions are marked by large symbols with white outlines. The small symbols show the distribution of stress axes within 95% confidence region. The black lines indicate major faults in Taiwan.

6. Discussion and conclusions

Based on the stress analysis of our new dataset, we found many interesting changes of stress fields in both space and time. Before the Chi-Chi earthquake, the trends of S_H at shallow depth of 0–10 km smoothly vary from 130° in the LV to 110° near the Coastal Plain in western Taiwan (Fig. 4). We suggest that this phenomenon is related to the oblique convergence between the EP and PSP at the LV of eastern Taiwan. The strike-slip movement is not only consumed by left-lateral motion on the LVF (Fig. 6A), as suggested in previous studies (Chung et al., 2008; Wu et al., 2006b, 2008b), but also is transferred into the Central Range, the Hsuehshan Range and possibly into the Western Foothills. This inference is justified by the gradual counterclockwise rotation of S_H between 22.5°N and 24°N from eastern to western Taiwan (Figs. 4A and 5A) as well as strike-slip faulting in the Hsuehshan Range and the Western Foothills (Fig. 6).

In southwestern Taiwan, the trends of S_H rotate about 20° to 30° anticlockwise at the depth range of 10–20 km with respect to those at shallow depths of 0–10 km (Fig. 4A and B). The distribution of seismicity and rotation of S_H in this region can be related to the Peikang Basement High (PKH, e.g. Meng, 1971; Mouthereau et al., 2002), a high-velocity barrier in western Taiwan as shown in tomography results (Wu et al., 2007) at depths between 10 and 20 km (Fig. 4B).

The orientations of S_H in the northern half of the Chi-Chi rupture area rotated 30° clockwise after the Chi-Chi earthquake (Fig. 7, Box *A*). The coseismic movement here is in the direction of 320-330°; while the pre-seismic motion is in the direction of 300° (Wu and Wu, 2007; Yu et al., 2001). We suggest that the S_H trends will gradually return to orientations in the pre- Chi-Chi period. This feature is also observed in seismicity changes (Wu and Chen, 2007). Before the Chi-Chi earthquake most of the earthquakes occurred in eastern Taiwan but shortly concentrated in western Taiwan after the Chi-Chi earthquake. Currently, most earthquake activities switch back to eastern Taiwan. However, the orientations of S_H in 2007 at the northern half of the Chi-Chi rupture area still differ by 30° from the pre-seismic orientations.

Significant changes of S_H orientations in the coseismic rupture area are inferred after the Chi-Chi earthquake in comparison with stationary S_H orientation to the south of the rupture zone. This suggests the stress level in the rupture area is of the same order of coseismic stress drop of about 10 MPa (Hwang et al., 2001) and the crustal strength on the fault zone is weak as indicated in Hsu et al. (2009b).

In addition to the preliminary stress analysis of this study, our complete focal mechanism dataset in Taiwan can also be applied to other studies involving geodynamic modeling, geological interpretations, and seismotectonics. We hope this dataset, as illustrated in the supplementary material will be useful to other colleagues of the society.

Supplementary materials related to this article can be foundonline at doi:10.1016/j.epsl.2010.07.047.

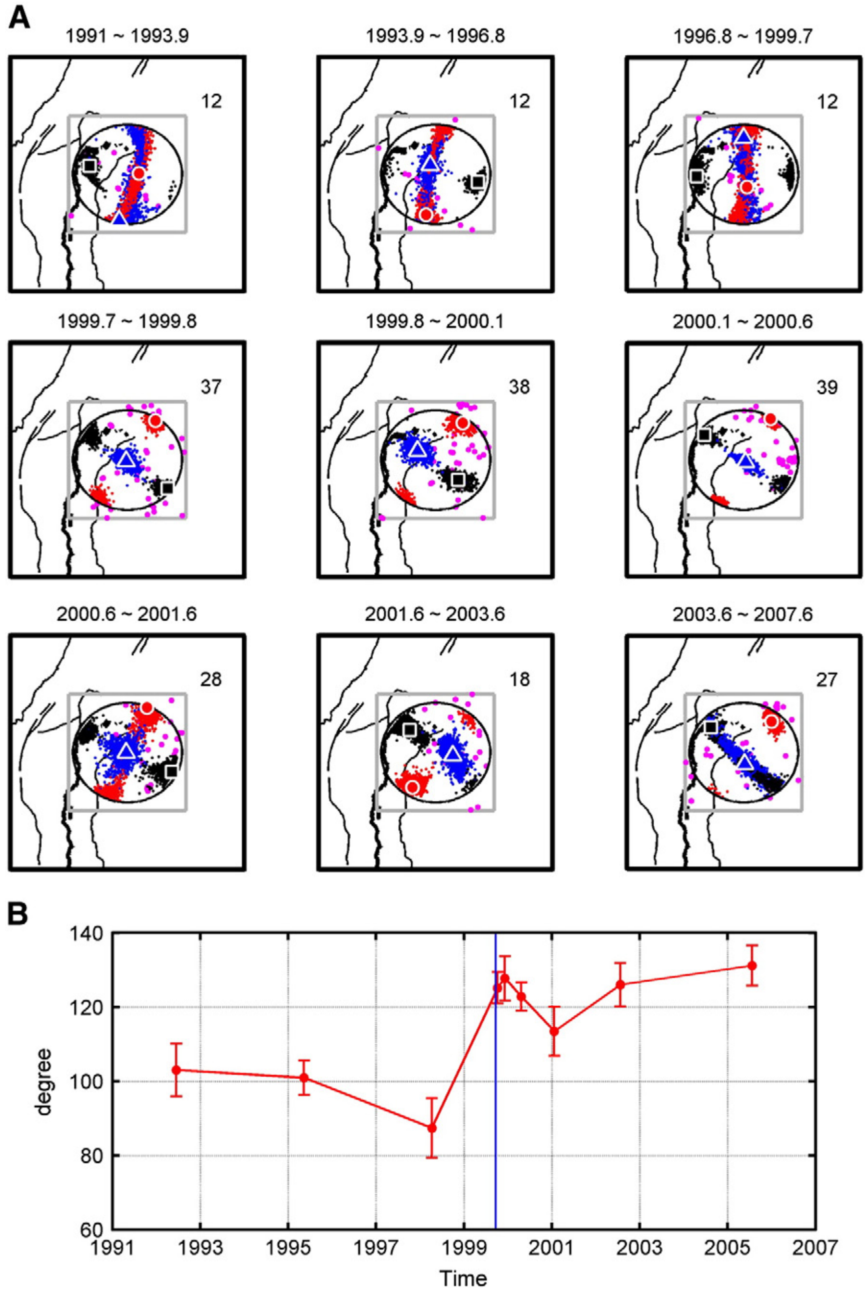

Fig. 7. Stress tensor inversions for Box *A* at nine periods shown on the top of each panel. (A) The top three panels and bottom six panels show stress axes before and after the Chi-Chi earthquake, respectively. Magenta dots indicate earthquake locations. Squares, triangles, and circles represent three principal stress axes, σ_1, σ_2 and σ_3, in equal-area projection of the lower hemisphere. The best solutions are marked by large symbols with white outlines. The small symbols show the distribution of stress axes within 95% confidence region. The black lines indicate major faults. The text denotes the number of focal mechanisms used in each period. (B) Temporal variations of orientations of S_H. Degrees are counted clockwise from the north. The blue line indicates the time of the Chi-Chi earthquake.

Acknowledgments

The authors wish to thank the Japan Meteorological Agency (JMA) for providing the arrival time data of JMA stations. This work was supported by the National Science Council (NSC) and Central Weather Bureau of the Republic of China.

References

Chang, S.H., Wang, W.H., 2006. Mechanical properties, slip and nucleation of the 1999 Chia-Yi earthquake: the question of static stress influence from the 1999 Chi-Chi earthquake. Terr. Atmos. Oceans Sci. 17 (2), 331–343.

Chang, C.H., Wu, Y.M., Shin, T.C., Wang, C.Y., 2000. Relocating the 1999 Chi-Chi earthquake, Taiwan. Terr. Atmos. Oceans Sci. 11 (3), 581–590.

Chang, C.H., Wu, Y.W., Zhao, L., Wu, F.T., 2007. Aftershocks of the 1999 Chi-Chi, Taiwan, earthquake: the first hour. Bull. Seismolog. Soc. Am. 97 (4), 1245–1258. doi:10.1785/0120060184.

Chen, K.C., Huang, B.S., Wen, K.L., Chiu, H.C., Yeh, Y.T., Cheng, S.N., Peng, H.Y., Chang, T.M., Shin, T.C., Shih, R.C., Lin, C.R., 1999. A study of aftershocks of the 17 July 1998 Ruey-Li, Chiayi earthquake. Terr. Atmos. Oceans Sci. 10 (3), 605–618.

Chen, H.Y., Kuo, L.C., Yu, S.B., 2004. Coseismic movement and seismic ground motion associated with the 31 March 2002 Hualien "331" earthquake. Terr. Atmos. Oceans Sci. 15 (4), 683–695.

Chen, C.C., Wang, W.C., Chang, Y.F., Wu, Y.M., Lee, Y.H., 2006. A correlation between the b-value and the fractal dimension from the aftershock sequence of the 1999 Chi-Chi, Taiwan, earthquake. Geophys. J. Int. 167 (3), 1215–1219. doi:10.1111/j.1365-246X.2006.03230.x.

Chen, Y.G., Kuo, Y.T., Wu, Y.M., Chen, H.L., Chang, C.H., Chen, R.Y., Lo, P.W., Ching, K.E., Lee, J.C., 2008. New seismogenic source and deep structures revealed by 1 the 1999 Chia-yi earthquake sequence in southwestern Taiwan. Geophys. J. Int. 172 (3), 1049–1054. doi:10.1111/j.1365-246X.2007.03686.x.

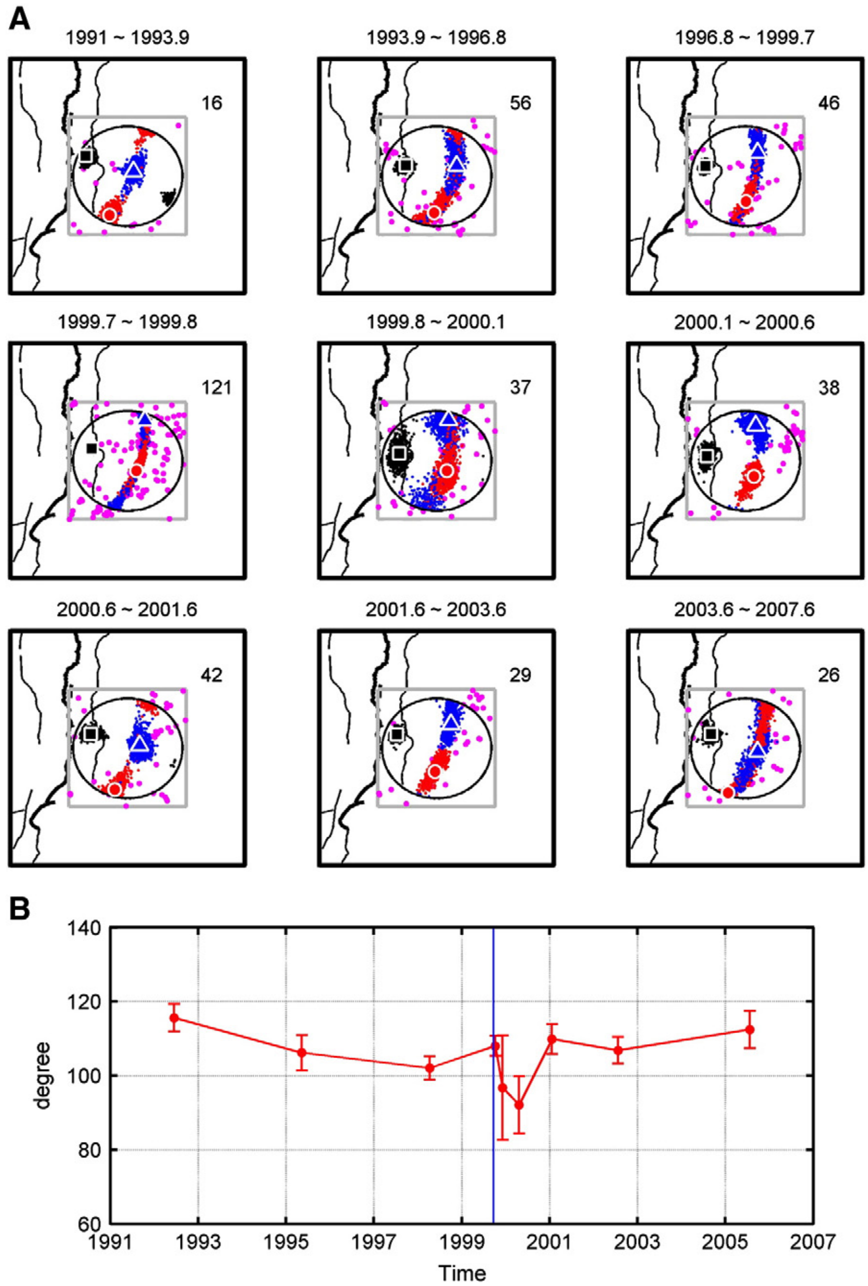

Fig. 8. Stress tensor inversions for Box *B* at nine periods shown on the top of each panel. (A) The top three panels and bottom six panels show stress axes before and after the Chi-Chi earthquake, respectively. Magenta dots indicate earthquake locations. Squares, triangles, and circles represent three principal stress axes, σ_1, σ_2 and σ_3, in equal-area projection of the lower hemisphere. The best solutions are marked by large symbols with white outlines. The small symbols show the distribution of stress axes within 95% confidence region. The black lines indicate major faults. The text denotes the number of focal mechanisms used in each period. (B) Temporal variations of orientations of S_H. Degrees are counted clockwise from north. The blue line indicates the time of the Chi-Chi earthquake.

Chen, H.Y., Hsu, Y.J., Lee, J.C., Yu, S.B., Kuo, L.C., Liu, C.C., Tsai, C.S., 2009. Coseismic displacements and slip distribution inferred from GPS and leveling observations for the 2006 Peinan Earthquake (Mw 6.1) in southeastern Taiwan. Earth Planets Space 61 (3), 299–318.

Chung, L.H., Chen, Y.G., Wu, Y.M., Shyu, J.B.H., Kuo, Y.T., Lin, Y.N.N., 2008. Seismogenic faults along the major suture of the plate boundary deduced by dislocation modeling of co-seismic displacements of the 1951 M7.3 Hualien-Taitung earthquake sequence in eastern Taiwan. Earth Planet. Sci. Lett. 269 (3–4), 416–426. doi:10.1016/j.epsl.2008.02.035.

Frohlich, C., 2001. Display and quantitative assessment of distributions of earthquake focal mechanisms. Geophys. J. Int. 144 (2), 300–308. doi:10.1046/j.1365-246x.2001.00341.x.

Hsu, Y.J., Yu, S.B., Simons, M., Kuo, L.C., Chen, H.Y., 2009a. Interseismic crustal deformation in the Taiwan plate boundary zone revealed by GPS observations, seismicity, and earthquake focal mechanisms. Tectonophysics 479 (1–2), 4–18. doi:10.1016/j.tecto.2008.11.016.

Hsu, Y.J., Avouac, J.P., Yu, S.B., Chan, C.H., Wu, Y.M., Woessner, J., 2009b. Spatio-temporal slip, and stress level on the faults within the western foothills of Taiwan: implications for fault frictional properties. Pure Appl. Geophys. 166 (10–11), 1853–1884. doi:10.1007/s00024-009-0510-5.

Hsu, Y.J., Yu, S.B., Chen, H.Y., 2009c. Coseismic and postseismic deformation associated with the 2003 Chengkung, Taiwan earthquake. Geophys. J. Int. 176 (2), 420–430. doi:10.1111/j.1365-246X.2008.04009.x.

Hu, J.C., Cheng, L.W., Chen, H.Y., Wu, Y.M., Lee, J.C., Chen, Y.G., Lin, K.C., Rau, R.J., Kuochen, H., Chen, H.H., Yu, S.B., Angelier, J., 2007. Coseismic deformation revealed by inversion of strong motion and GPS data: the 2003 Chengkung earthquake in eastern Taiwan. Geophys. J. Int. 169 (2), 667–674. doi:10.1111/j.1365-246X.2007.03359.x.

Huang, C.Y., Yuan, P.B., Tsao, S.J., 2006. Temporal and spatial records of active arc-continent collision in Taiwan: a synthesis. Bull. Geol. Soc. Am. 118 (3–4), 274–288. doi:10.1130/B25527.1.

Hwang, R.D., Wang, J.H., Huang, B.S., Chen, K.C., Huang, W.G., Chang, T.M., Chiu, H.C., Tsai, C.C., 2001. Estimates of stress drop of the Chi-Chi, Taiwan, earthquake of 20 September 1999 from near-field seismograms. Bull. Seismolog. Soc. Am. 91 (5), 1158–1166. doi:10.1785/0120000708.

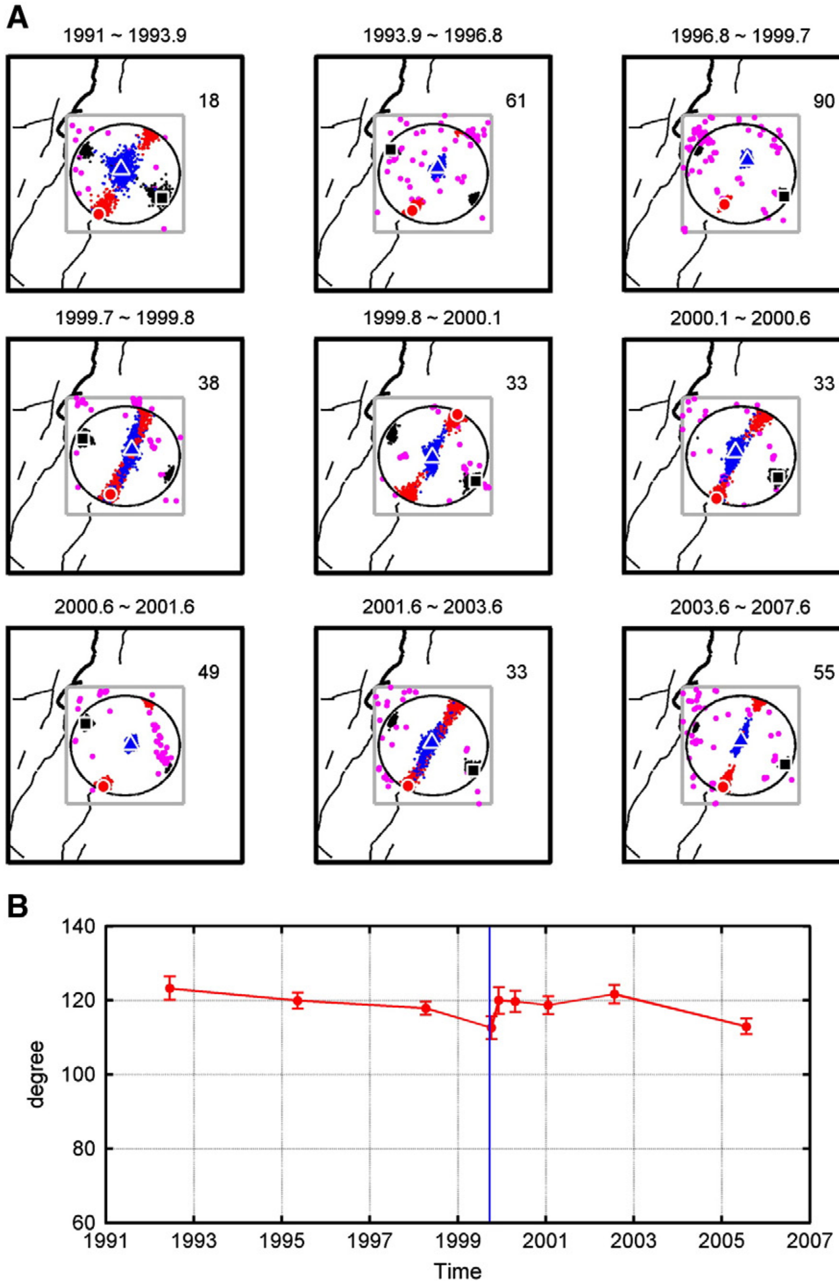

Fig. 9. Stress tensor inversions for Box *C* at nine periods shown on the top of each panel. (A) The top three panels and bottom six panels show stress axes before and after the Chi-Chi earthquake, respectively. Magenta dots indicate earthquake locations. Squares, triangles, and circles represent three principal stress axes, σ_1, σ_2 and σ_3, in equal-area projection of the lower hemisphere. The best solutions are marked by large symbols with white outlines. The small symbols show the distribution of stress axes within 95% confidence region. The black lines indicate major faults. The text denotes the number of focal mechanisms used in each period. (B) Temporal variations of orientations of S_H. Degrees are counted clockwise from north. The blue line indicates the time of the Chi-Chi earthquake.

Kao, H., Shen, S.S.J., Ma, K.F., 1998. Transition from oblique subduction to collision: earthquakes in the southernmost Ryukyu arc—Taiwan region. J. Geophys. Res. 103 (B4), 7211–7229.

Lund, B., Townend, J., 2007. Calculating horizontal stress orientations with full or partial knowledge of the tectonic stress tensor. Geophys. J. Int. 170 (3), 1328–1335. doi:10.1111/j.1365-246X.2007.03468.x.

Meng, G.Y., 1971. A conception of the evolution of the island of Taiwan and its bearing on the development of the western Neogene sedimentary basin. Petrol. Geol. Taiwan 9, 241–258.

Michael, A.J., 1984. Determination of stress from slip data—faults and folds. J. Geophys. Res. 89 (NB13), 1517–1526.

Michael, A.J., 1987. Use of focal mechanisms to determine stress—a control study. J. Geophys. Res. 92 (B1), 357–368.

Mouthereau, F., Deffontaines, B., Lacombe, O., Angelier, J., 2002. Variations along the strike of the Taiwan thrust belt: basement control on structural style, wedge geometry, and kinematics. Geol. Soc. Am. Spec. Pap. 358, 35–58.

Mozziconacci, L., Angelier, J., Delouis, B., Rau, R.J., Bethoux, N., Huang, B.S., 2009. Focal mechanisms and seismotectonic stress in North Central Taiwan in relation with the Chi-Chi earthquake. Tectonophysics 466 (3–4), 409–426. doi:10.1016/j.tecto.2007.11.003.

Perfettini, H., Avouac, J.P., 2004. Postseismic relaxation driven by brittle creep: a possible mechanism to reconcile geodetic measurements and the decay rate of aftershocks, application to the Chi-Chi earthquake, Taiwan. J. Geophys. Res. 109 (B2), B02304. doi:10.1029/2003JB002488.

Shin, T.C., Teng, T.L., 2001. An overview of the 1999 Chi-Chi, Taiwan, earthquake. Bull. Seismolog. Soc. Am. 91 (5), 895–913. doi:10.1785/0120000738.

Shin, T.C., Tsai, Y.B., Yeh, Y.T., Liu, C.C., Wu, Y.M., 2003. Strong-motion instrumentation programs in Taiwan. In: Lee, W.H.K., Kanamori, H., Jennings, P.C. (Eds.), Handbook of Earthquake and Engineering Seismology. Academic Press, pp. 1057–1602.

Teng, L.S., 1990. Geotectonic evolution of late Cenozoic arc-continent collision in Taiwan. Tectonophysics 183 (1–4), 57–76.

Teng, T.L., Tsai, Y.B., Lee, W.H.K., 2001. Preface to the 1999 Chi-Chi, Taiwan, earthquake dedicated issue. Bull. Seismolog. Soc. Am. 91 (5), 893–894. doi:10.1785/0120000700.

Tsai, Y.B., Teng, T.L., Chiu, J.M., Liu, H.L., 1977. Tectonic implications of the seismicity in the Taiwan region. Mem. Geol. Soc. Chin. 2, 13–41.

Wu, Y.M., Chen, C.C., 2007. Seismic reversal pattern for the 1999 Chi-Chi, Taiwan, Mw 7.6 earthquake. Tectonophysics 429 (1–2), 125–132. doi:10.1016/j.tecto.2006.09.015.

Wu, Y.M., Chiao, L.Y., 2006. Seismic quiescence before the 1999 Chi-Chi, Taiwan Mw7.6 earthquake. Bull. Seismolog. Soc. Am. 96, 321–327.

Wu, Y.M., Wu, C.F., 2007. Approximate recovery of coseismic deformation from Taiwan strong-motion records. J Seismolog. 11 (2), 159–170. doi:10.1007/s10950-006-9043-x.

Wu, Y.M., Chang, C.H., Hsiao, N.C., Wu, F.T., 2003. Relocation of the 1998 Rueyli, Taiwan, earthquake sequence using three-dimension velocity structure with stations corrections. Terr. Atmos. Oceans Sci. 14 (4), 421–430.

Wu, Y.M., Chen, Y.G., Shin, T.C., Kuochen, H., Hou, C.S., Hu, J.C., Chang, C.H., Wu, C.F., Teng, T.L., 2006a. Coseismic vs. interseismic ground deformations, faults rupture inversion and segmentation revealed by 2003 Mw 6.8 Chengkung earthquake in eastern Taiwan. Geophys. Res. Lett. 33, L02312. doi:10.1029/2005GL024711.

Wu, Y.M., Chen, Y.G., Chang, C.H., Chung, L.H., Teng, T.L., Wu, F.T., Wu, C.F., 2006b. Seismogenic structure in a tectonic suture zone: with new constraints from 2006 Mw6.1 Taitung earthquake. Geophys. Res. Lett. 33 (2), L22305. doi:10.1029/2006GL027572.

Wu, Y.M., Chang, C.H., Zhao, L., Shyu, J.B.H., Chen, Y.G., Sieh, K., Avouac, J.P., 2007. Seismic tomography of Taiwan: improved constraints from a dense network of strong-motion stations. J. Geophys. Res. 112 (B8), B08312. doi:10.1029/2007JB004983.

Wu, Y.M., Chang, C.H., Zhao, L., Teng, T.L., Nakamura, M., 2008a. A comprehensive relocation of earthquakes in Taiwan from 1991 to 2005. Bull. Seismolog. Soc. Am. 98 (3), 1471–1481. doi:10.1785/0120070166.

Wu, Y.M., Zhao, L., Chang, C.H., Hsu, Y.J., 2008b. Focal mechanism determination in Taiwan by genetic algorithm. Bull. Seismolog. Soc. Am. 98 (2), 651–661. doi:10.1785/0120070115.

Wu, Y.M., Shyu, J.B.H., Chang, C.H., Zhao, L., Nakamura, M., Hsu, S.K., 2009a. Improved seismic tomography offshore northeastern Taiwan: implications for subduction and collision processes between Taiwan and the southernmost Ryukyu. Geophys. J. Int. 178 (2), 1042–1054. doi:10.1111/j.1365-246X.2009.04180.x.

Wu, Y.M., Chang, C.H., Zhao, L., Hsiao, N.C., Chen, Y.G., Hsu, S.K., 2009b. Relocation of the 2006 Pingtung earthquake sequence and seismotectonics in Southern Taiwan. Tectonophysics 479 (1–2), 19–27. doi:10.1016/j.tecto.2008.12.001.

Yu, S.B., Chen, H.Y., Kuo, L.C., Lallemand, S.E., Tsien, H.H., 1997. Velocity field of GPS stations in the Taiwan area. Tectonophysics 274 (1–3), 41–59.

Yu, S.B., Kuo, L.C., Hsu, Y.R., Su, H.H., Liu, C.C., Hou, C.S., Lee, J.F., Lai, T.C., Liu, C.C., Liu, C.L., 2001. Preseismic deformation and coseismic displacements associated with the 1999 Chi-Chi, Taiwan, earthquake. Bull. Seismolog. Soc. Am. 91 (5), 995–1012.